Design and Optimization of a Steering Geometry for a Micromobility Vehicle

Peter Krönes, Adrian Brune, Prof. Dr.-Ing. Lars Mikelsons
University of Augsburg, Chair of Mechatronics, 86159 Augsburg, Germany
(peter.kroenes@uni-a.de)

Abstract

In pursuit of making urban traffic more sustainable and efficient, micromobility vehicles can be a possibility for extending public local transport. To solve some of the problems of the currently widespread rental e-scooters, a partially autonomous solution is being considered. The autonomy is intended only for redistribution and independent charging. For autonomous operation, a stable vehicle is necessary, which leads to the extension to three wheels. The resulting increased complexity of the steering will be addressed in this article. The relevant chassis characteristics will be discussed, and on this basis, an optimization of a novel steering mechanism will be performed.

1 Introduction

Due to increasing urbanization, urban mobility concepts are facing significant challenges [1]. The infrastructure is not designed for current demands, and in most European cities, it cannot be structurally modified to meet today's needs. To find a solution, a greater expansion of public transportation is essential. However, this often fails to fully meet individual needs, as public transit cannot cover the start and end points for every individual. In recent years, the micromobility concept of e-scooters has emerged as a solution in many major cities, where they are distributed throughout the city and can be booked via an app. Yet, this solution introduces its own set of problems. The distribution of vehicles does not meet demand, currently compensated for by an oversupply. Vehicles with low battery levels are manually collected, charged, and redistributed, which, aside from requiring significant labor, also worsens the CO2 footprint of the vehicles [2]. Additional issues arise from users who leave the vehicles in inconvenient locations, thereby blocking driveways, bike paths, stairs, etc. The vehicles are also subject to vandalism, which in some cases can cause extensive ecological damage.

1.1 Semi-Autonomous Micromobility Vehicles

A potential solution to these issues could be semi-autonomous micromobility vehicles [3]. These vehicles are designed to be operated like conventional e-scooters but can also move independently. This allows for a demand-driven distribution within the urban area, eliminating the need for an oversupply. Additionally, it enables the vehicles to autonomously travel to charging stations, clear pathways if they have been left in inconvenient locations, and partly disappear from the cityscape outside peak usage times, which also helps to reduce vandalism.

1.2 Vehicle requirements

The semi-autonomy requires a stable platform; hence the concept includes a front axle with two unpowered wheels and one powered rear wheel. To ensure ride comfort and safety, the front wheels are equipped with suspension. This introduces a level of complexity to the chassis that necessitates a specific steering design. Additionally, a novel steering concept is to be integrated, which allows not only the conventional rotation of the handlebar but also a tilting motion to control the steering.

2 Vehicle Suspension

For optimizing steering parameters, we have to discuss the vehicles wheel suspension parameters. In this case we have a double wishbone suspension that is usually defined like seen in **Figure 1**. All mentioned parameters and how they have been altered for the simplified suspension of the scooter are listed below. The final setup that is used for the optimization can be seen in **Figure 2**.

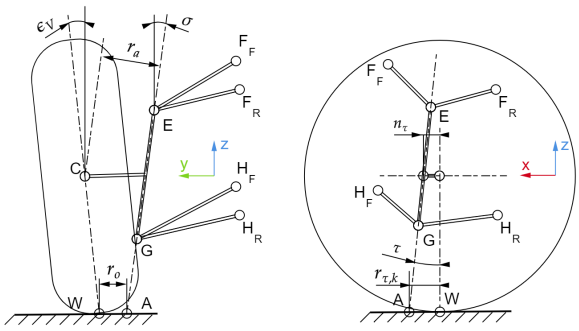

Figure 1 Standard parameters of a wheel suspension defined by Matschinsky[4]. Graphic based on [5].

Camber Angle ε_V: Camber angle is used to increase the tire contact area of the leading wheel (outer wheel relative to the curve) while cornering. Since our scooter has wheels with a much narrower contact patch than a car and therefo-

DOI: 10.17185/duepublico/81695

re has arguably no loss in contact area while cornering, the camber angle has been set to zero.

Kingpin Inclination σ: With kingpin inclination the vehicle is lifted according to the wheel steering angle. Since the vehicles mass is working against the lift of the steering, the vehicle automatically pulls straight with no steering input. Mainly for simplifying the geometry, the kingpin inclination has also been set to zero.

Caster Angle τ: When the caster angle is positive, meaning the top of the steering axis is tilted towards the rear of the vehicle, it creates a situation where the steering axis intersects the ground ahead of the contact point of the tire. As the vehicle moves forward, the force of the ground on the tire generates a torque around the steering axis due to this offset. This torque rotates the wheels back to their straight-ahead position. For our scooter the caster angle has been set to zero.

Scrub Radius r_0: The scrub radius acts as a lever arm on which bumps can act on to affect the steering wheel feedback. Therefore, it mainly affects handling characteristics and driver's comfort. Since the kingpin inclination is zero the scrub radius is restricted by the wheel itself. It has been designed to be as small as physically possible.

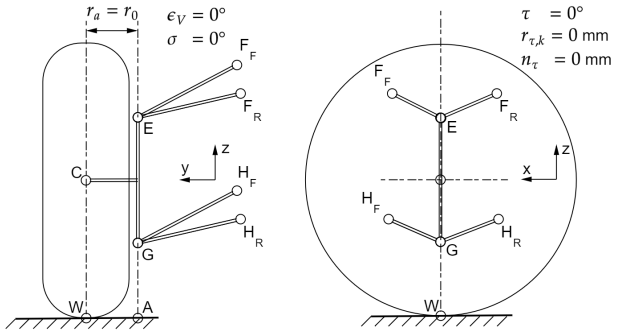

Figure 2 Parameters of the scooters suspension in rear view on the left and side view on the right. **Note:** For a clearer representation of all parts, the wishbone struts were not shown overlapping on the rear view.

Both front wheels have a shock absorber that is mounted on the lower wishbone and goes through the upper wishbone to its mounting point as shown in **Figure 3**. The steering optimization is done with the shock absorber 30 % compressed.

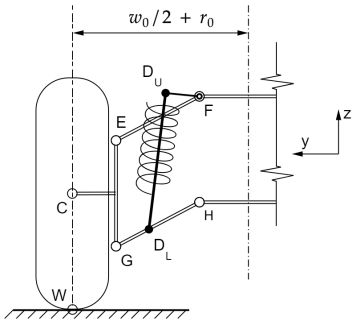

Figure 3 Suspension setup in rear view, with shock absorber with 30 % sag.

3 Vehicle Steering Mechanism

The steering mechanism is designed to be either used by tilting the steering bar around an axis parallel to the vehicle's x-axis or by rotating the steering bar around its z-axis. With adding the steering by tilting to the vehicle, it gains the ability to be steered by leaning into curves while the rotation can still achieve higher wheel angles to achieve a sufficient turning circle for autonomous operation on sidewalks. To clarify how both steering modes work, left side of **Figure 4** shows the conventional steering by turning the handle bar by $\theta_z = 10°$ while the right sight shows steering by tilting the handle bar by $\theta_x = 10°$.

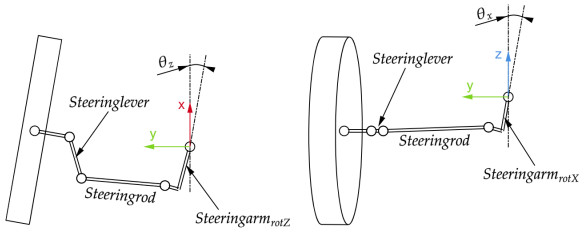

Figure 4 Left side: Steering by rotating the handle bar in top view.
Right side: Steering by tilting the handle bar in rear view.

A rendered image of all parts in a position where both steering modes are actuated and all joints have their respective degrees of freedom visualized can be seen in **Figure 5**.

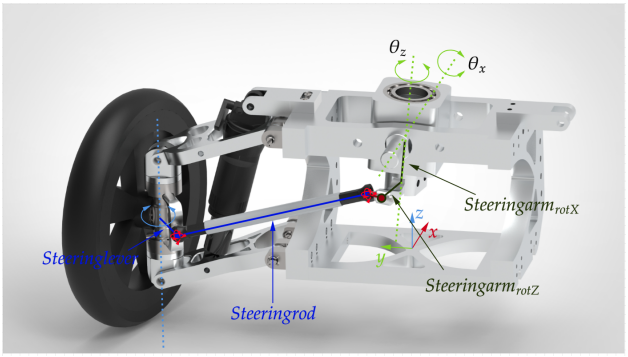

Figure 5 Rendering of the current vehicle setup with all Steering related parts labeled. The degrees of freedom of all joints are visualized.

4 Evaluation criteria for steering mechanisms

For an optimization we need criteria that are measurable and not a matter of own preference. We picked the turning circle and the ackermann condition to optimize the steering parameters.

4.1 Ackermann Condition

The Ackermann condition (or Ackermann steering geometry) pertains to the ideal steering design that allows the inner and outer wheels to turn at the appropriate angles during a turn. According to the Ackermann principle, in a turn, the inner wheel needs to turn at a sharper angle than the outer wheel because it has a smaller radius to cover. This principle reduces tire slip and wear during turns, improving handling and efficiency [6]. The Ackermann condition is met when the extensions of the front wheels' axes intersect at the rear axle as seen in **Figure 6**. If the intersection point is, for example, behind it, the minimum distance to the rear axle is defined as the Ackermann error err_A. To obtain a value that is comparable across different vehicle lengths, the ratio is given relative to the vehicle's wheelbase. Therefore a steering mechanism that meets the ackermann condition perfectly is defined as 100 % Ackermann and parallel steering is defined as 0 % Ackermann:

$$rat_A = \left(\frac{T}{T + err_A}\right) \cdot 100 \tag{1}$$

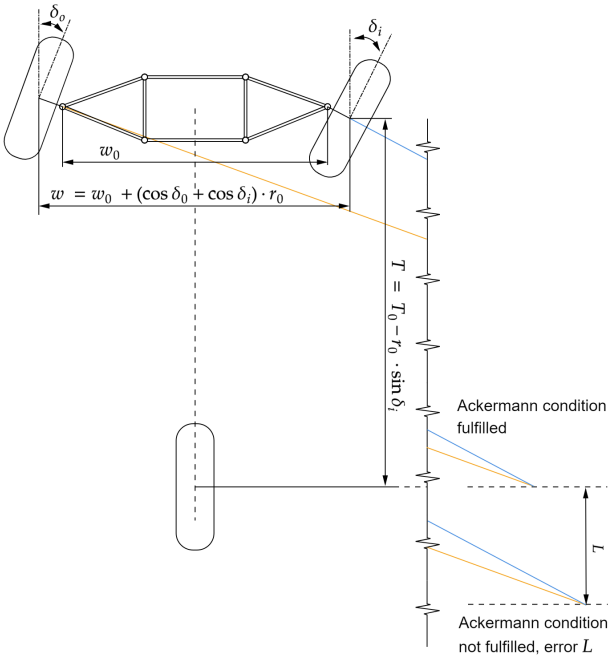

Figure 6 Vehicle in top view with depiction of the Ackermann error.

4.2 Turning Radius

The turning radius is a critical measure of a vehicle's maneuverability. It refers to the smallest circular turn (or the smallest U-turn) that the vehicle can make. A smaller turning radius indicates better maneuverability, allowing the vehicle to navigate tight spaces more effectively. It's a particularly important measure for vehicles intended for urban environments, where narrow streets are common. The turning radius is defined as following:

$$r_T = \frac{T}{\sin\delta_o} \tag{2}$$

5 Optimization

The main objective is to minimize the Ackermann error. As the actual calculation of err_A is very long and purely geometrical, it is not presented in detail. The optimization is run over steering input angles that have been presumed to be the range that is used in such vehicles, currently there is no close match to compare to and this might have to be adapted at a later stage of development. The constriction on the steering mechanism parts result from design space limitations for example a steering rod longer than $w_0/2$ would collide with the wheel.

$$\min_{\theta_x,\theta_z} \quad \mathrm{err}_A(\theta_x,\theta_z) \tag{3}$$

$$\text{s.t.} \quad 0^\circ \le \theta_x \le 10^\circ \tag{4}$$

$$0^\circ \le \theta_z \le 35^\circ \tag{5}$$

$$Steeringrod < w_0/2 \tag{6}$$

$$100\,\mathrm{mm} \le Steeringlever \le 250\,\mathrm{mm} \tag{7}$$

$$20\,\mathrm{mm} \le Steeringarm_{rotX} \le 100\,\mathrm{mm} \tag{8}$$

$$50\,\mathrm{mm} \le Steeringarm_{rotZ} \le 150\,\mathrm{mm} \tag{9}$$

$$r_T \le 2600\,\mathrm{mm} \tag{10}$$

Since the steering mechanism is designed in a way that it will inevitably reach a singularity it has to be checked if the singularity occurs in the predefined range of motion.
For the Optimization the programming language Julia [7] is used. The Optimization problem is formulated in the modeling language for mathematical optimization JuMP [8], using the Interiot Point optimizer [9].

6 Result

In our selected vehicle configuration and within the defined optimization constraints, we have identified an optimal solution characterized by an absolute Ackermann error of less than 700 mm. This performance metric was observed across steering inputs ranging from $\theta_z = 0^\circ$ to 35° and $\theta_x = 0^\circ$ to 10°, as depicted in **Figure 7**. Furthermore, the relative Ackermann error across these specified angles is detailed in **Figure 8**. Analysis of both figures reveals that the largest Ackermann error occurs near a steering input of 0°, whereas optimal steering performance is achieved within the 5° to 20° range for θ_z. Within this interval, the steering input θ_x significantly influences the Ackermann error. Conversely, outside this range, variations in θ_x appear to

exert negligible impact on steering accuracy.

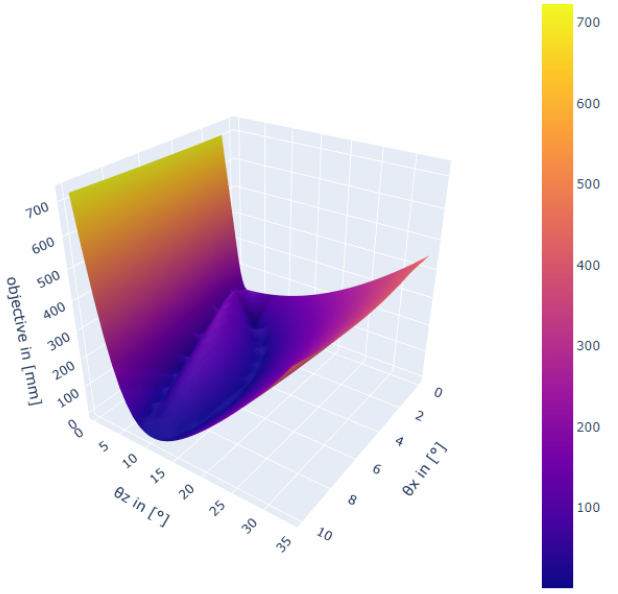

Figure 7 Absolute Ackermann error over input steering angles θ_x and θ_y.

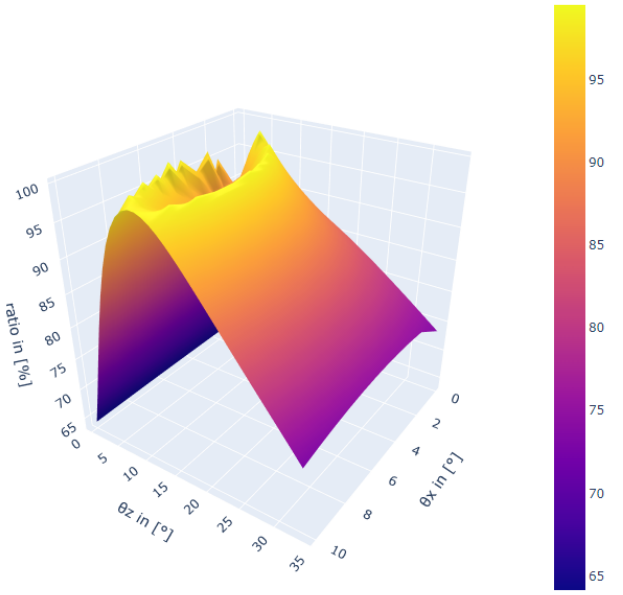

Figure 8 Relative Ackermann error in % over input steering angles θ_x and θ_y.

To more closely investigate the regions exhibiting larger Ackermann errors, we analyzed the angles of the inner (δ_i) and outer (δ_o) wheels relative to the optimal angle according to the Ackermann condition (δ_a). Consistent with previous observations, the steering input θ_x exerts a negligible influence on areas with heightened Ackermann error. Consequently, we explored a plot showcasing δ_i, δ_o, and δ_a across a range of $\theta_z = 0°$ to $35°$, at fixed $\theta_x = 0°$ (**Figure 9**) and $\theta_x = 10°$ (**Figure 10**). This analysis revealed that the absolute error in wheel angle remains minimal at lower steering inputs and begins to increase noticeably beyond a steering input of $\theta_z = 25°$. Thus, we infer that the most significant impact on tire wear and handling occurs at higher wheel angles, typically associated with lower speeds, suggesting that such effects should be less perceptible.

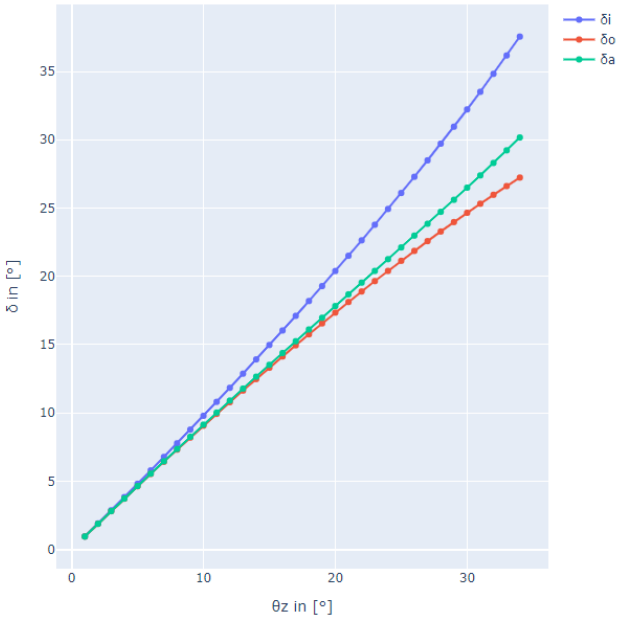

Figure 9 Steering angle of inner wheel δ_i with optimal angle of outer wheel δ_a and real angle of optimized geometry δ_o over θ_z from $0°$ to $35°$ at $\theta_x = 0$.

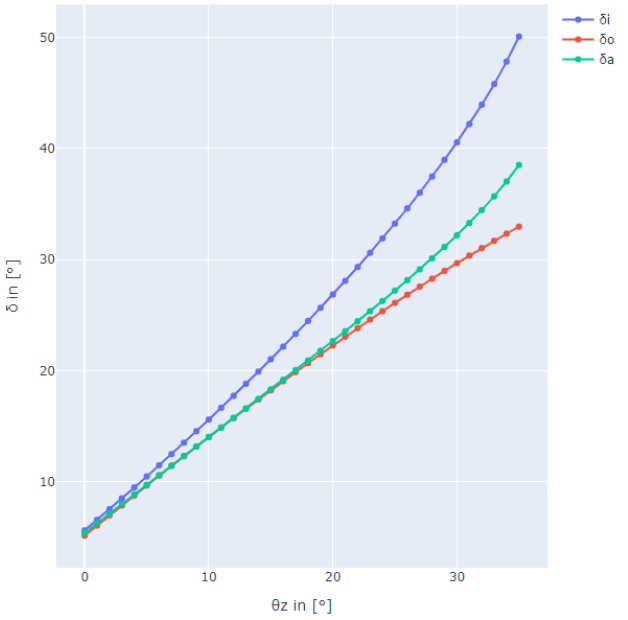

Figure 10 Steering angle of inner wheel δ_i with optimal angle of outer wheel δ_a and real angle of optimized geometry δ_o over θ_z from $0°$ to $35°$ at $\theta_x = 10$.

A critical aspect of assessing steering geometry is ensuring that wheel angles are increasing strictly monotonically with respect to increases in either steering input. The adherence of our optimized parameter set to this criterion is illustra-

ted in **Figure 11**, where the resultant steering angle of the inner wheel (δ_i) is plotted as a function of both θ_x and θ_z. Notably, this plot also highlights the maximum wheel angle, correlating to a turning radius of 2.551 m.

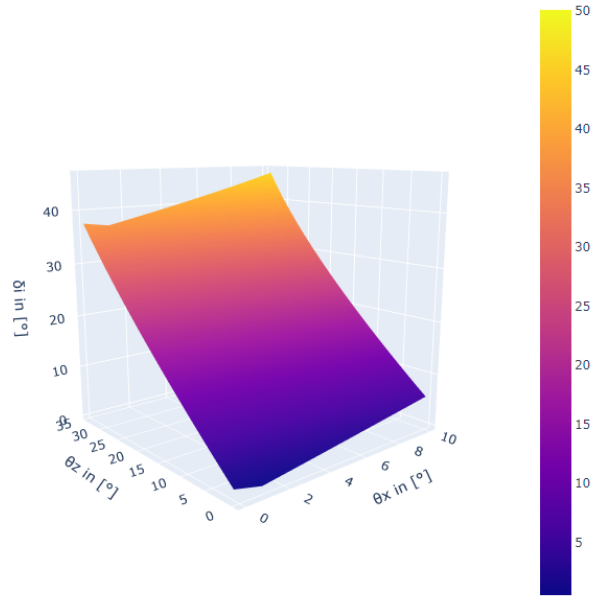

Figure 11 Resulting steering angle δ_i of optimized geometry.

7 Conclusion

A new steering mechanism specialized for semi-autonomous micromobility vehicles has been developed, with a focus on optimizing parameters to closely align with the Ackermann condition. The optimization efforts have led to promising results, demonstrating that the steering mechanism consistently achieves over 65% Ackermann compliance across all steering angles, indicating a high level of performance in various driving scenarios. This performance is noteworthy, especially considering the challenges in making direct comparisons due to the unique size of the vehicles in question. For context, a study by Veneri et al. [6] comparing different steering geometries in race cars found Ackermann ratios ranging from 30% to 50%.

8 Future Work

The subsequent phase involves conducting tests on a vehicle prototype equipped with the newly developed steering mechanism. This step is crucial for gaining a deeper insight into the impact of specific steering and wheel suspension configurations on this vehicle type, and to determine the perceptibility and relevance of these effects. Additionally, the interaction between road feedback and the steering mechanism will be thoroughly evaluated.

Literatur

[1] Philipp Rode. “Trends and Challenges: Global Urbanisation and Urban Mobility”. In: *Megacity Mobility Culture*. Lecture Notes in Mobility. Berlin, Heidelberg: Springer Berlin Heidelberg, 2013, pp. 3–21. ISBN: 978-3-642-34734-4. DOI: 10.1007/978-3-642-34735-1_1.

[2] Joseph Hollingsworth, Brenna Copeland, and Jeremiah X. Johnson. “Are e-scooters polluters? The environmental impacts of shared dockless electric scooters”. In: *Environmental Research Letters* 14.8 (2019), p. 084031. DOI: 10.1088/1748-9326/ab2da8.

[3] Lennart Luttkus, Peter Krönes, and Lars Mikelsons. *Scoomatic: Simulation and Validation of a Semi-Autonomous Individual Last-Mile Vehicle*. 2020. DOI: 10.17185/DUEPUBLICO/71204.

[4] Wolfgang Matschinsky. *Radführungen der Straßenfahrzeuge: Kinematik, Elasto-Kinematik und Konstruktion*. 3., aktualisierte u. erw. Aufl. Berlin [u.a.]: Springer, 2007. ISBN: 978-3-540-71197-1.

[5] Peter Pfeffer and Manfred Harrer. *Lenkungshandbuch*. Vieweg+Teubner, 2011. ISBN: 978-3-8348-0751-9.

[6] M. Veneri and M. Massaro. “The effect of Ackermann steering on the performance of race cars”. In: *Vehicle System Dynamics* 59.6 (2021), pp. 907–927. ISSN: 0042-3114. DOI: 10.1080/00423114.2020.1730917.

[7] Jeff Bezanson et al. “Julia: A Fresh Approach to Numerical Computing”. In: *SIAM Review* 59.1 (2017), pp. 65–98. ISSN: 0036-1445. DOI: 10.1137/141000671.

[8] Iain Dunning, Joey Huchette, and Miles Lubin. “JuMP: A Modeling Language for Mathematical Optimization”. In: *SIAM Review* 59.2 (2017), pp. 295–320. ISSN: 0036-1445. DOI: 10.1137/15M1020575.

[9] Andreas Wächter and Lorenz T. Biegler. “On the implementation of an interior-point filter line-search algorithm for large-scale nonlinear programming”. In: *Mathematical Programming* 106.1 (2006), pp. 25–57. ISSN: 0025-5610. DOI: 10.1007/s10107-004-0559-y.

DOI: 10.17185/duepublico/81695
URN: urn:nbn:de:hbz:465-20240304-104643-9